Cleaner Energy Systems 6 (2023) 100087

Contents lists available at ScienceDirect

Cleaner Energy Systems

journal homepage: www.elsevier.com/locate/cles

Experimental investigation, modeling and in-situ monitoring of a gas-driven absorption heat pump in Belgium

Camila Dávila *, Javier Vega, Vincent Lemort

University of Liège, Thermodynamics Laboratory, Liège, Belgium

ARTICLE INFO

Keywords:
Gas absorption heat pump
Experimental results
Field results
Heat pump performance
Heat pump modeling

ABSTRACT

This work describes the methodology used to realize a performance analysis of an ammonia-water condensing gas absorption heat pump. This heat pump shows a nominal heating output of 18,9 kW for an outdoor temperature of 7 °C and a delivery temperature of 35 °C, and it is designed for domestic hot water and heating production. The experimental results obtained in the laboratory are contrasted with those obtained from the monitoring of two residential facilities in the northern part of Belgium. Experimental tests were carried out in a climatic chamber to emulate different outdoor climatic conditions based on a combination of the EN 12309 requirements and typical Belgium weather data. Measurements of gas consumption, electrical consumption, water flows, and temperatures were collected to compute performance indicators. On the other hand, the monitoring data was analyzed and contrasted with the experimental results to evaluate the field systems' performance; the problems found and modifications made are described and discussed. The results show that the performance of the systems is highly dependent on the coupling with other appliances, on the operating conditions and control of the system, resulting in penalties that can be considerable depending on the configuration used. An empirical model calibrated with experimental data is proposed, as well as a penalization factor calibrated with the monitoring data. The results presented evidence the differences found between the studied facilities, highlighting the main role of proper installation and control not to diminish the main performance indicators.

Introduction

International commitments related to energy use, environmental impact, and decarbonization goals are increasingly restrictive and ambitious. In most scenarios, electrification is one of the key milestones, combined with the effects of smart control systems, more efficient buildings, technologies, and changes in consumer behaviors.

It is not possible, however, to electrify everything in the short term. Today half of the energy demand in buildings in Europe was used for space and water heating, with fossil fuels covering 60 % of this heating energy demand in 2021 (International Energy Agency, 2022). In the world, natural gas is the most commonly used fuel for heating, representing 42 % of the total share in buildings, and its demand increases in every World Energy Model scenario over the next five years (Stated Policies Scenario *STEPS*, Announced Pledges Scenario *APS*, Net Zero Scenario *NZE*), diverging afterward due to many factors depending on countries and regions (International Energy Agency, 2022; International Energy Agency, 2021).

In this context, the building sector has been pointed out as one of the key areas in the matter; in 2017, the household sector represented 30 % of the final energy consumption in the European Union (EU) with a total of 288 million tons of oil equivalent (Mtoe), only being surpassed by the industrial sector (European Environment Agency, 2020). According to 2016 data, the energy consumption in dwellings in Belgium destinated just to space and water heating represented 1.52 Mtoe (European Environment Agency, 2016), where the consumption of natural gas represented 45.6 % of the total energy consumption followed by electricity consumption (29.7 %), solid fuel consumption (22.4 %) and petroleum products (9.4 %) (European Environment Agency, 2013). Other studies also suggest that the use phase in technologies that provide space heating and domestic hot water in Europe contributes to more than 97 % of the total environmental impact of the appliance (Famiglietti et al., 2021).

Heat pumps appear as an interesting topic since they are a more efficient technology compatible with residential applications. Studies have shown that heat pumps are a good alternative to reduce energy

* Corresponding author.
E-mail address: cdavila@uliege.be (C. Dávila).

https://doi.org/10.1016/j.cles.2023.100087
Received 20 December 2022; Received in revised form 27 April 2023; Accepted 22 September 2023
Available online 23 September 2023

consumption and CO_2 emissions (Aste et al., 2013; Blarke, 2012; Chua et al., 2010). Also, it is a market that is undoubtedly growing: between 2005 and 2018, the use of heat pumps in the heating sector in the EU represented an increase in energy consumption of 8.3 Mtoe, surpassed only by the use of solid biomass (European Environment Agency, 2020). Government policies and private sector strategies point, in the short term, to an increase in the market share of heat pump technologies (International Energy Agency, 2022; International Energy Agency, 2022).

An attractive alternative to traditional appliances are gas absorption heat pumps (GAHP) since it offers substantial cost and energy savings compared to conventional commercially available systems for water heating (Keinath and Srinivas, 2017). It also presents an alternative to reduce the peak demand on the electrical grid produced by the use of electric heat pumps (Hommelberg et al., 2022) and opens the door to the use of alternative fuels such as hydrogen-enriched natural gas (International Energy Agency, 2022).

At (Fumagalli et al., 2017), an standardization method for monitored heat pumps that includes the type of use, system configuration and technology is proposed; different system boundaries are defined, showing that the performance of the system is not only determined by the efficiency of the heat pump but that is highly dependent on the correct integration, sizing, and control of the system to not negatively affect the COP. In particular, the monitored systems that were more affected in their efficiency were the ones that did not work on steady state conditions, what is usually the consequence of an oversized system for the thermal demand requirements.

On the other hand, several studies have been done to compare different gas-driven heat pumps considering their components, the system thermodynamic cycle, control strategies, and parameters such as delivery water temperature and gas input, arriving to complex and detailed models (Babak Dehghan et al., 2020; Wu et al., 2020) that aimed to provide realistic results for different applications and operational conditions where no experimental data is available. Different control and optimization strategies are applied, resulting in optimal design and control guidelines for the proposed cases. Some GAHP models are experimentally calibrated (Aprile et al., 2017; Aprile et al., 2016), but the amount of data available is far from being representative, appealing to linear interpolations and extrapolations to cover a higher range of operating conditions; also, the research interest is in the cycle itself and control strategies, having the appliance as boundary and not taking into account the integration of the system into real applications.

This work seeks to compare the behavior of the same system under controlled operating conditions in the laboratory and field facilities. The differences found in the performances are discussed and quantified. The results allows to perform a empirical model calibrated with experimental data that includes operation condition variables such as delivery water temperature, outdoor temperature and part load working capacity; the model allows to compute performance indicators such as the COP, as well as the heating capacity, gas heat input and electrical input. The penalties related to operation under ideal and real conditions are taken into account by including a penalization factor in the model, calibrated with the monitoring data, that is related to the operating conditions in the field, the quality of the installation and the coupling with other heat generation systems.

Description of the system

Designed for space heating (SH) and domestic hot water (DHW) for residential applications, the tested gas absorption heat pump (GAHP) has a nominal heating capacity of 18.9 kW. The system is based on the Water-Ammonia absorption cycle using outdoor air as renewable energy source (low-temperature heat source) and natural gas combustion as high-temperature heat source; the delivered hot water is the medium-temperature heat sink. The working principle of the system is represented in the diagram shown in Fig. 1.

To heat the absorbent-refrigerant solution in the Generator (GEN), a Burner (BRN) driven by natural gas is used. The heat delivered to the GEN causes the separation of the two components of the solution by desorption. The desorbed ammonia vapor leaves the GEN and passes through the Rectifier (REC) to remove the last parts of water that could remain. Then it continues to the Condenser (COND), transferring the heat of the refrigerant to the water destinated to the Heating Circuit (HC) e.g., radiators, floor heating, or others. The water is previously Pre-Heated in a heat exchanger (PH) by the combustion gases and driven by the Water Circulation Pump (WP).

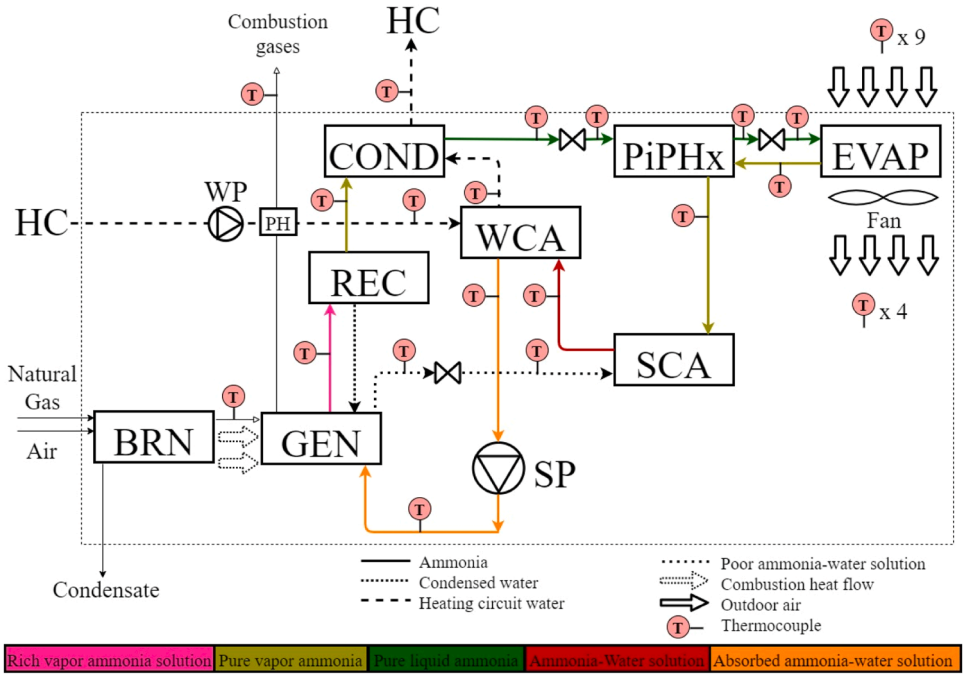

Fig. 1. Gas absorption heat pump working principle scheme.

To reduce its pressure, the refrigerant leaving the COND is throttled by means of a restrictor valve and cooled down inside the Pipe in Pipe heat exchanger (PiPHx); then, by means of a second restrictor valve, is brought to the ideal pressure and temperature conditions before entering the Evaporator (EVAP) where the liquid refrigerant is evaporated by taking heat from the surrounding air. Then, the low-pressure vapor ammonia is overheated in the PiPHx before being sent to the Solution Cooled Absorber (SCA), where it meets the poor refrigerant solution coming from the GEN whose pressure is reduced by a third restrictor valve. Here, a first absorption stage takes place, having as result an ammonia-water solution with traces of vapor ammonia.

Since the absorption process is an exothermic reaction, the solution coming from the SCA is sent to the Water Cooled Absorber (WCA) where a considerable amount of thermal energy is transferred to the water of the heating circuit. Here the vapor ammonia absorption process is completed, and the solution is pumped back to the GEN using a Solution Pump (SP) where the cycle starts again.

Description of the test bench

The system is an outdoor unit, thus, it is installed and the tests are performed in a climatic chamber to vary and control the temperature and humidity conditions. The test bench facilities are shown in Fig. 2.

The appliance needs to be supplied by electricity and natural gas, consumptions that are measured. To emulate the heat demand of a house, a heat exchanger is placed in the room adjacent to the climate chamber where the load is regulated by controlling the chilled-water flow rate through the exchanger by means of the valve V1. The products derived from the operation of the system such as combustion gases and condensate are removed from the test bench; the hot water produced is sent to the HC loop to fulfill the heat demand.

The room temperature is decreased by means of an outdoor air-to-water heat pump unit located inside the chamber. The humidity of the room is reduced by water condensation in the evaporators of both units and drawn out of the chamber. Once the temperature and humidity setpoints are reached, a steady state is maintained by means of an electrical heater and a humidifier. These latter are connected to an acquisition system and controlled by a PI controller which receives the signal of temperature and humidity sensors placed at the entrance of the evaporator.

In terms of measuring devices, inside the heat pump, only surface thermocouples were installed on the different pipes between the components. These thermocouples were placed on an electro-insulating and thermo-conductive sheet, fixed with plastic clamps, and insulated at each measurement point to ensure thermal contact and correctly measure the fluid temperature. On the rest of the test bench, in-pipe thermocouples were used. In the cases where the temperature of a large cross-section had to be measured, a grid of thermocouples was used; more precisely, 4 equidistant thermocouples were installed at the fan exhaust and 9 at the evaporator supply. Measurements of gas consumption, water consumption, electrical consumption, room temperature, and humidity are also collected.

For caution and since the unit works with an ammonia-water solution that is harmful to health, an ammonia sensor was installed close to the unit to detect leaks and a release pipe was installed to extract the ammonia out of the room if necessary. The measuring devices and their characteristics are summarized in Table 1.

Table 1
Measuring devices.

Sensor	Type	Accuracy
Thermocouples	*T*	±0.3 K
Humidity	Capacitive–wettable	±2 %
Water meter	Volumetric	±2 % Q_n; ±5 % Q_{min}
	Magnetic	±0.5 % from 0.3 to 11.89 m/s
Gas meter	Diaphragm	±0.5 %
Power meter	Multifunctional	±0.5 %
Ammonia sensor	Electrochemical	±5 ppm

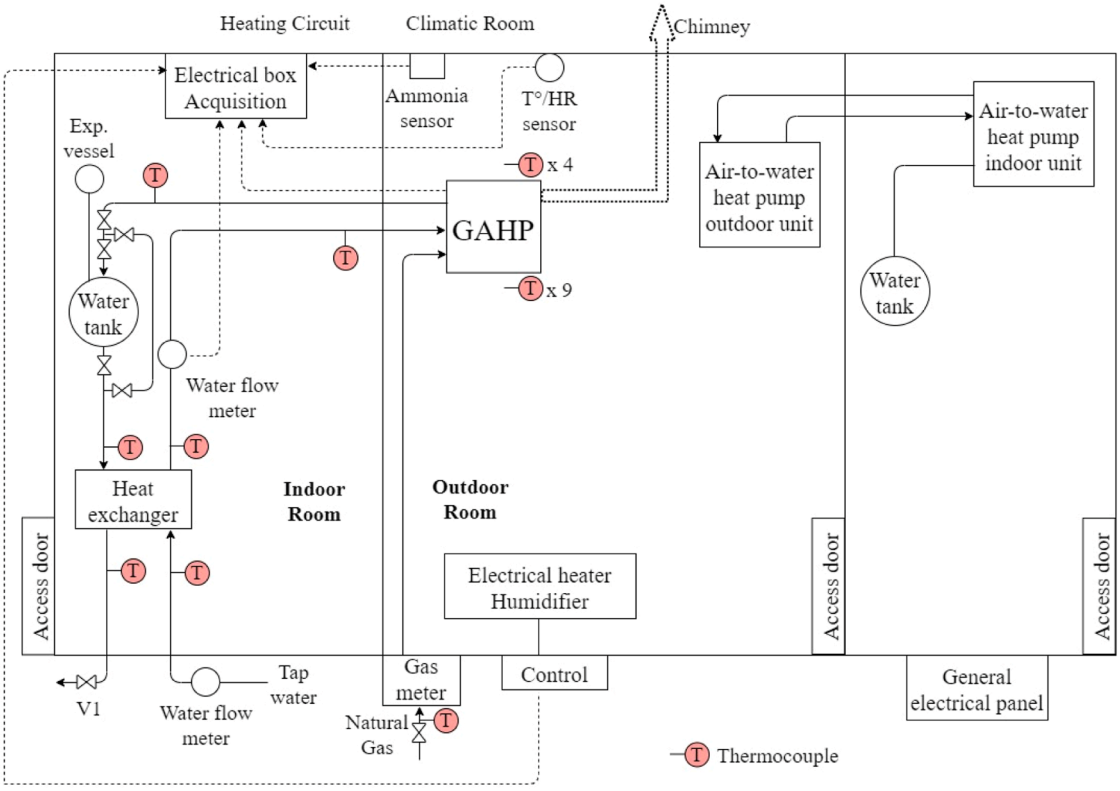

Fig. 2. Schematic of the test bench used to characterize the absorption heat pump.

Testing conditions

The gas absorption heat pump has certain operating parameters that are supplied by the manufacturer and some of these are modifiable. A display board gives access to different menus and to facilitate the characterization of the system, some of them are changed as described hereunder.

First, it is sought to maintain a constant water temperature difference between the delivery and the inlet of the appliance. To achieve this, the modulation of the circulation pump is activated and the water delta T° is set to 10 K.

Second, it is necessary to set the permissible delivery and return water temperature range of the appliance not to restrict the system's behavior. In other words, a wide enough water temperature range allows it to not operate, for example, at partial load. Therefore, the delivery water temperature range is set between 30 °C and 75 °C, while the return range goes between 20 °C and 30 °C.

Third, the control method of the delivery water temperature should be set. This can be done by a variable water setpoint which depends on the outdoor temperature (weather-compensated control) or by means of a fixed setpoint. The latter method is used, coinciding with the maximum delivery water temperature set (75 °C) and having the option of modifying it if necessary.

Finally, it is possible to establish a heating capacity control of the system allowing the modulation of the burner or based on an "On/Off" behavior. The first option is chosen, having as a consequence a modulation of the gas flow rate on the burner side, while in the absorption cycle it is reflected in variations in the fan and water circulation pump drive voltage.

The described adjustable parameters configuration is shown in Table 2.

The performed test matrix is shown in Table 3. The test campaign is based on the EN 12309 (European Standards, 2014) regarding the test conditions at full load concerning the type of appliance (e.g., air-to-water, water-to-water), its application (e.g., low/medium/high temperature), the outdoor heat exchanger conditions referring to dry-wet bulb temperatures and the classification of the climate (e.g., medium, warm, or cold).

To consider the weather conditions to which the appliances are subjected in the field in terms of temperature and humidity, a weather data analysis was made for the cold season from October 2018 to March 2019 based on two local weather stations close to systems (Weather Underground, 2020).

Based on these two aspects, the performed test matrix is shown in Table 3. Here, five outdoor air-dry bulb temperatures and four water delivery temperatures are considered. This base matrix is performed for a relative humidity of 75 % since it is the most frequent value obtained from the weather data analysis. Every test is performed at full load on a steady state for a period of 20 min. The test conditions are monitored throughout the test with the test bench acquisition system, and also with a smartphone connected to the appliance to verify the data; the manufacturer application allows to have real time information, such as operation temperatures, current heating capacity output, activation of defrost cycles, among others, based on the internal sensors of the appliance.

Table 2
Adjustable parameters configuration.

Description	Setting
Modulation of the circulation pump	Active
Heating circuit water ΔT° setpoint	10 K
Delivery water temperature range	From 30 °C to 75 °C
Return water temperature range	From 20 °C to 30 °C
Delivery water temperature setpoint	75 °C
Heating capacity modulation	Active

Table 3
Gas absorption heat pump test matrix.

		Water delivery temperature [°C]			
		35	45	55	65
Outdoor dry bulb Temp. [°C]	12 7 2 −7 −10	75 %			

Monitoring

The system is installed in two residential houses in the northern part of Belgium. The two houses are considered to be in the same climatic region. These installations have sensors that provide information equivalent to the one obtained in the laboratory to analyze the system's inputs and outputs, allowing to estimate efficiencies. The data collected with a sampling rate of five minutes is daily sent to the Cloud for later analysis.

The sites named Brasschaat and Brecht are equally monitored. The used sensors are identical between sites and are placed at the same indoor spots, as can be seen in the installation schemes shown in Figs. 3 and 4, respectively.

Both installations have sensors to measure indoor and outdoor ambient conditions, as well as gas and electric meters to measure the consumption of the system. A heat meter is installed between the inlet and outlet pipes of the machine to measure the heating energy delivered by the system based on the measurement of the water flow that circulates through the heating circuit and its respective inlet and outlet temperatures.

The monitored houses count with water tanks for domestic hot water and heat storage. In both sites, the space heating is provided by radiators. Additionally, Brasschaat site has thermal solar panels and an extra buffer for DHW storage, adding complexity to the installation. The heat produced by the gas absorption heat pump is directed towards one or the other tank depending on whether the demand is for SH or DHW. Two temperature probes control the behavior of the appliance at Brasschaat (numbers 1 and 2), while at Brecht only one probe is used (number 1).

The hydraulic pipelines are properly insulated to avoid thermal losses. The distance between the system and the indoor room is less than one meter, with the temperature sensor's placed one meter farther away from the wall. The system and sensors installation has been carried out and approved by the manufacturer; no leakages has been detected after installation not during the period of operation and monitoring of the system. This last point is verified thanks to the error history recorded by the system, to which the manufacturer has access through the control panel.

The sensors references, their precision and resolution of the acquired data are presented in Table 4.

It is worth mentioning that some control and internal parameters of the systems such as heating capacity modulation or temperature setpoint are not remotely controlled or monitored. This means that changes or modifications made by the user or installer could not be communicated, being difficult or impossible to identify only with the data analysis. A constant monitoring is carried out, without guaranteeing that no omissions occurred that could potentially affect the monitoring data and its subsequent analysis.

Results and discussion

Laboratory

A valid data collection period is defined on the European standard based on the coefficient of change shown in Eq. (1). If this coefficient remains within 2.5 % during the data collection period, then the test can

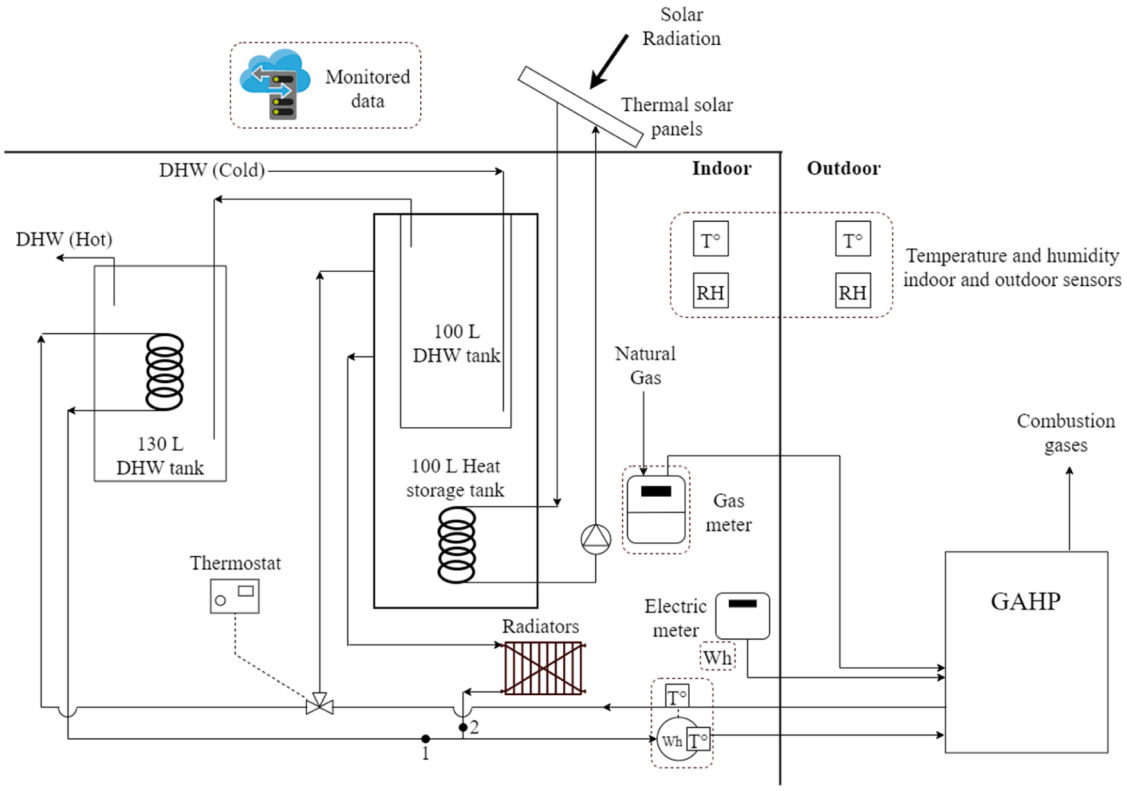

Fig. 3. Installation scheme of Brasschaat monitoring site.

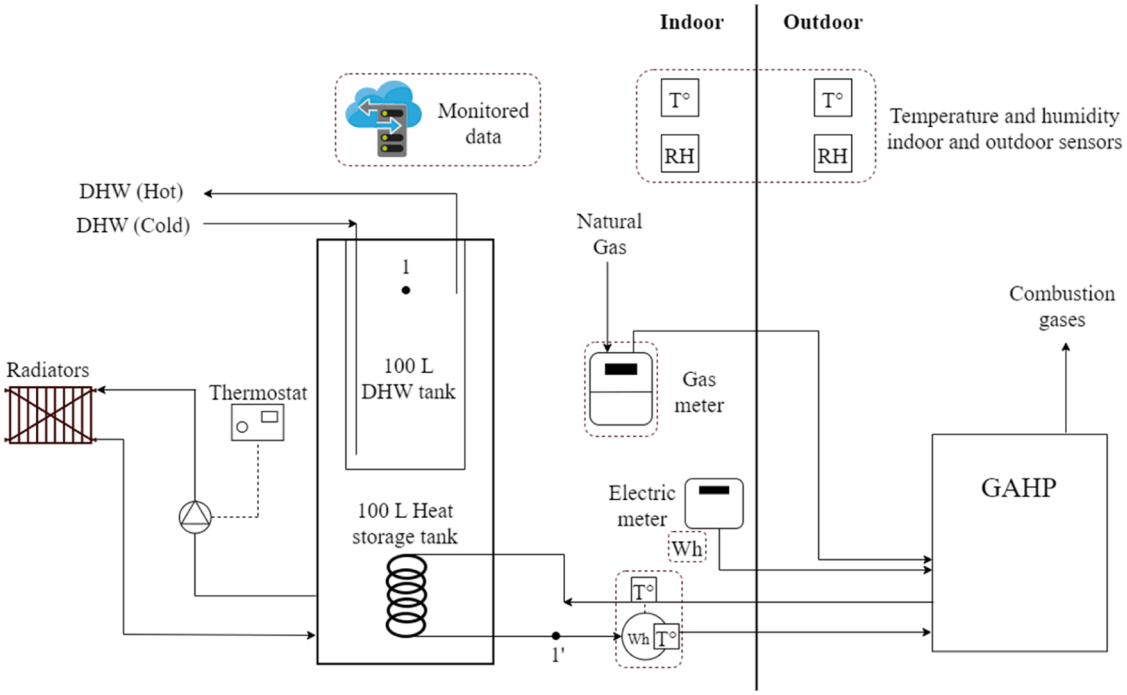

Fig. 4. Installation scheme of Brecht monitoring site.

be considered as steady state. This coefficient is the difference between the outlet and the inlet temperatures of the heat transfer medium at the indoor room heat exchanger and should be calculated every 5 min starting at the end of the previous period ($\tau = 0$).

$$\%\Delta T = \frac{\Delta T_{i(\tau=0)} - \Delta T_{i(\tau)}}{\Delta T_{i(\tau=0)}} * 100 \quad (1)$$

where $\%\Delta T$ is the coefficient of change, in %; $\Delta T_{i(\tau=0)}$ is the average difference between the outlet and the inlet temperatures for the first 5 min period; $\Delta T_{i(\tau)}$ is the average difference between the outlet and the

Table 4
Sensors used at monitored sites.

Sensor	Reference	Resolution *	Precision
External temperature and humidity	Weptech Munia	0,1 K 0,1 %	±0,3 K ±2 %
Internal temperature and humidity	Weptech Munia	0,1 K 0,1 %	±0,3 K ±2 %
Heat counter	Qalcosonic E1	1 kWh 1 L 0,1 K	Accuracy Class 2 (OIML R 49-1, 2006)
Machine electrical energy counter	Iskraemeco ME162	1 Wh	Accuracy Class 1 (IEC 62053-21, 2003)
Gas volume counter	Elster BK-G4T	10 L	<1 %
Data logger (cloud connection)	Viltrus MX-9	–	–

* Data logger included.

inlet temperatures for another 5-min period than the first 5 min.

In addition, allowable deviation values from the set values are established. This corresponds to ±0.3 K for room temperature, ±2 % for room mean humidity and ±1 K from the setpoint for the depart water temperature.

The COP_{global} of each test was estimated as the ratio of the heating capacity output to heat and electric power input as defined in Eq. (2). The COP_{Th} and COP_{El} are defined in the same way in Eqs. (3) and (4), only taking into account the respective input.

$$COP_{global} = \frac{\dot{Q}_{HC}}{\dot{Q}_{gas} + \dot{W}_{in}} \tag{2}$$

$$COP_{Th} = \frac{\dot{Q}_{HC}}{\dot{Q}_{gas}} \tag{3}$$

$$COP_{El} = \frac{\dot{Q}_{HC}}{\dot{W}_{in}} \tag{4}$$

The heating capacity output corresponds to that given to the heating circuit $\dot{Q}_{HC}$ while the inputs are the thermal heat rate obtained from the natural gas combustion $\dot{Q}_{gas}$ and the electric input to the appliance $\dot{W}_{in}$. The heat transfer rate transferred to the heating circuit water is defined in Eq. (5).

$$\dot{Q}_{HC} = \dot{Q}_{WCA} + \dot{Q}_{cond} + \dot{Q}_{gases} \tag{5}$$

where $\dot{Q}_{WCA}$, $\dot{Q}_{cond}$ and $\dot{Q}_{gases}$ are the heat transfer rates obtained from the water cooled absorber, the condenser, and the combustion gases, respectively.

Since the internal configuration of the system makes it difficult to install sensors between components that allow measuring the previously defined heat inputs individually, it is decided to measure the heating capacity output of the appliance transferred to the heating circuit water as shown in Eq. (6).

$$\dot{Q}_{HC} = \dot{m}_{HC,w} * c_{p,w} * (T_{out} - T_{in}) \tag{6}$$

where $\dot{m}_{HC,w}$ is the heating circuit water flow, $c_{p,w}$ is the specific heat of water, T_{out} and T_{in} are the outlet and inlet water temperatures of the system. Similarly, the heat input is defined in Eq. (7).

$$\dot{Q}_{gas} = \dot{V}_{gas} * HCV \tag{7}$$

where $\dot{V}_{gas}$ is the consumed gas flow and HCV is the daily average high calorific value. This value is calculated by the natural gas company according to the ISO 6974 by a chromatographic analysis at the metering station at 15 bar and 11 °C. The supplied values are corrected as indicated in (Paulus and Lemort, 2022), resulting in a reduction of 0.13 % of the value provided.

The electric consumption of the appliance $\dot{W}_{in}$ is constantly registered and considered in the results, with maximum variations of 2 % between tests and close to 0.35 kW. This consumption includes components such as the fan, oil pump, water circulation pump, and internal sensors.

With these considerations, the results obtained for the test matrix for the COP_{global} are shown in Table 5; for COP_{Th} and COP_{El}, the results are summarized in Tables 6 and 7. The results are computed meeting the requirements of Eq. (1) and are based on the average values of the measurements carried out during 20 min for each test.

The results obtained in the laboratory confirm the expected trends, with a global performance that increase as the ambient temperature does, and decreases if the water outlet temperature increases; the same is observed for the thermal capacity. The performance penalty due to the electrical consumption it is observed in Table 6, representing between 2 and 4 points of the COP_{global}.

Monitoring

Both sites were exhaustively monitored during 2020 and 2021. Their monthly COP_{global} for the whole year based on the high calorific value are shown in Fig. 5.

A clear seasonal effect can be observed, showing a penalty in the COP_{global} during summer that is related to the fact that the systems are less frequently used and no SH is required, generating more on/off cycles to supply only the production of DHW. In this sense, a greater impact is observed in Brasschaat site. This can be partially explained by the coupling of the thermal solar panels and their effect on the working temperature, inducing a change in the behavior of the system. However, these results are far from the ones expected and obtained in the laboratory, especially for winter conditions. Even more, unexpected large differences are observed between the performances of both machines.

To try to explain the differences with Tables 5, 6 and 7, an in-depth analysis of the behavior of both systems was carried out. Fig. 6 shows the daily thermal production of both sites in relation to their COP_{global} during 2020. Even though Brecht produces more thermal energy compared to Brasschaat, the system is less efficient.

On the other hand, the daily thermal production is related to the way in which the production of the system is controlled (i.e., On/Off or modulation). Since this information is unknown and is not part of the data collected from the monitoring, a deeper look to try to establish a relationship between the smoothness of the behavior of the system and the electrical consumption is made in Fig. 7. Here, Brecht has a higher

Table 5
COP_{global} and Thermal Capacity values at a relative humidity of 75 %.

COP_{global}		T° delivery			
		35	45	55	65
Outdoor T°	12	1.45 ± 0.05	1.34 ± 0.05	1.19 ± 0.05	1.05 ± 0.04
	7	1.38 ± 0.05	1.29 ± 0.05	1.13 ± 0.04	1.04 ± 0.04
	2	1.36 ± 0.05	1.21 ± 0.05	1.09 ± 0.04	0.95 ± 0.04
	−7	1.21 ± 0.05	1.13 ± 0.04	1.02 ± 0.04	0.86 ± 0.03
	−10	1.16 ± 0.04	1.14 ± 0.04	0.95 ± 0.04	0.86 ± 0.03
Th. capacity [kW]		T° delivery			
		35	45	55	65
Outdoor T°	12	21.11 ± 0.79	19.31 ± 0.74	16.98 ± 0.66	14.82 ± 0.58
	7	19.55 ± 0.77	18.57 ± 0.71	16.30 ± 0.64	14.92 ± 0.59
	2	20.10 ± 0.78	18.01 ± 0.69	15.64 ± 0.61	13.70 ± 0.54
	−7	18.33 ± 0.69	16.89 ± 0.64	15.13 ± 0.59	12.65 ± 0.50
	−10	17.36 ± 0.65	16.82 ± 0.63	14.14 ± 0.55	12.66 ± 0.50

Table 6
COP_{Th} values at a relative humidity of 75 %.

COP_{Th} 75 %		$T°$ delivery			
		35	45	55	65
Outdoor $T°$	12	1,48 ± 0.06	1,38 ± 0.05	1,22 ± 0.05	1,08 ± 0.04
	7	1,41 ± 0.06	1,32 ± 0.05	1,16 ± 0.05	1,06 ± 0.04
	2	1,39 ± 0.05	1,24 ± 0.05	1,12 ± 0.04	0,98 ± 0.04
	−7	1,24 ± 0.05	1,16 ± 0.04	1,05 ± 0.04	0,89 ± 0.04
	−10	1,18 ± 0.04	1,17 ± 0.04	0,98 ± 0.04	0,88 ± 0.04

Table 7
COP_{El} values at a relative humidity of 75 %.

COP_{El} 75 %		$T°$ delivery			
		35	45	55	65
Outdoor T°	12	60.32 ± 2.27	55.17 ± 2.13	48.51 ± 1.90	42.35 ± 1.68
	7	55.86 ± 2.22	53.05 ± 2.04	47.94 ± 1.90	42.62 ± 1.69
	2	57.42 ± 2.26	51.45 ± 1.97	44.69 ± 1.75	39.16 ± 1.56
	−7	52.38 ± 1.99	48.25 ± 1.83	43.24 ± 1.69	36.15 ± 1.44
	−10	49.60 ± 1.88	48.07 ± 1.82	40.41 ± 1.57	36.16 ± 1.43

electrical consumption, thus the machine is working for a longer amount of time which could be related to a smoother behavior; this information though is not conclusive to explain the differences found.

It is noticed that the working temperature of both systems is different as can be seen in Fig. 8 for year 2020. Here, the distribution of the depart and return temperatures of both monitored systems is summarized, where the mid line corresponds to the median of the dataset.

It is observed that the working operation temperature range of both sites is wide. This is normal for the return temperatures towards the system due to the fact that it evolves according to the way in which the heating circuit is progressively heated. Nevertheless, the depart temperature distribution in Brasschaat is more narrow than in Brecht, where the latter works with a depart water temperature regime of 5 K higher than the former, what could explain the differences between sites.

The presented results show that the systems are not as efficient as expected in the field, thus, an intervention is performed in situ on July 2021 to verify the installation of the systems and their parameters configuration.

As a result of these interventions it was found that in both sites the gas valve was wrongly set for the type of gas, what affects the reliability of the system. Furthermore, not enough gas was being burned in Brecht affecting the performances; the system was configurated to work with rich gas while in reality it was lean gas, causing the gas consumption to be lower due to the parameter used and resulting in a lower thermal output.

On the other hand, the error log in Brecht registered many "On/Off" cycles due to the fact that the circulation pump of the appliance was incorrectly wired to the control board; besides, the temperature probe that controls the modulation of the system based on the return water temperature was misplaced on the hydraulic circuit (point 1 in Fig. 4 instead of the point 1′). This caused that the return water temperatures to the system to be high, forcing the unit to decrease its heating capacity output to the minimum possible (about 60 %) and affecting the COP. The reduction of the heating capacity to the minimum occurs when the $\Delta T°$ between the depart and return temperatures of the system is less than the 10 K set.

The results of the interventions on the previously shown indicators can be seen comparing Figs. 9 and 12, were the vertical line points out the time of the modifications made on site. A few percentual points of improvement can be observed for both sites for the monthly COP_{global} after intervention, raising in Brasschaat above 1; Brecht on the other hand, remains close to 0.9 as maximum monthly value but improving also its monthly values.

Despite this small monthly increase in the COP_{global}, Figs. 10 and 11 show the differences between the production and consumption before and after intervention, approaching the results of both facilities, decreasing the data dispersion and explaining the differences between sites. Now the thermal daily production in Brasschaat is clearly higher than the one in Brecht; this added to the similar electrical daily consumption in both sites, the better performance results from one site relative to the other one are much clearer.

The contrast between Figs. 8 and 12 evidences the improvements made in Brecht in terms of depart and return water temperatures; in contrast, no major effect can be observed in Brasschaat.

This is explained by the fact that, as show in Fig. 3, the thermal production in Brasschaat is dispatched to the circuit that requires it by means of a 3-way valve, allowing a better control of the appliance be means of two control probes (1 and 2); since the control probes were

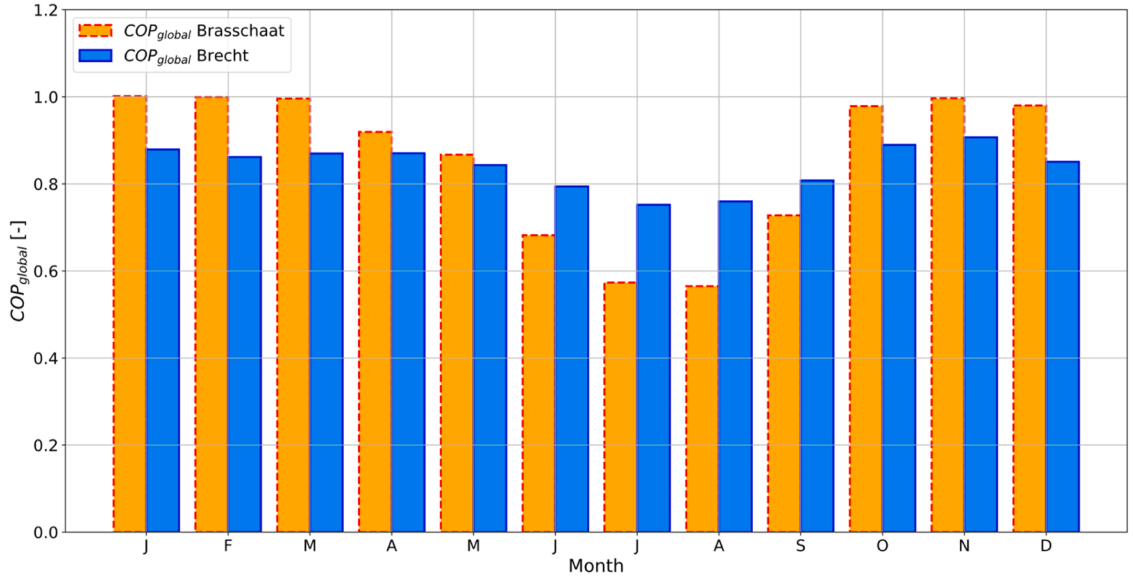

Fig. 5. Monitored GAHP's monthly COP_{global} during 2020.

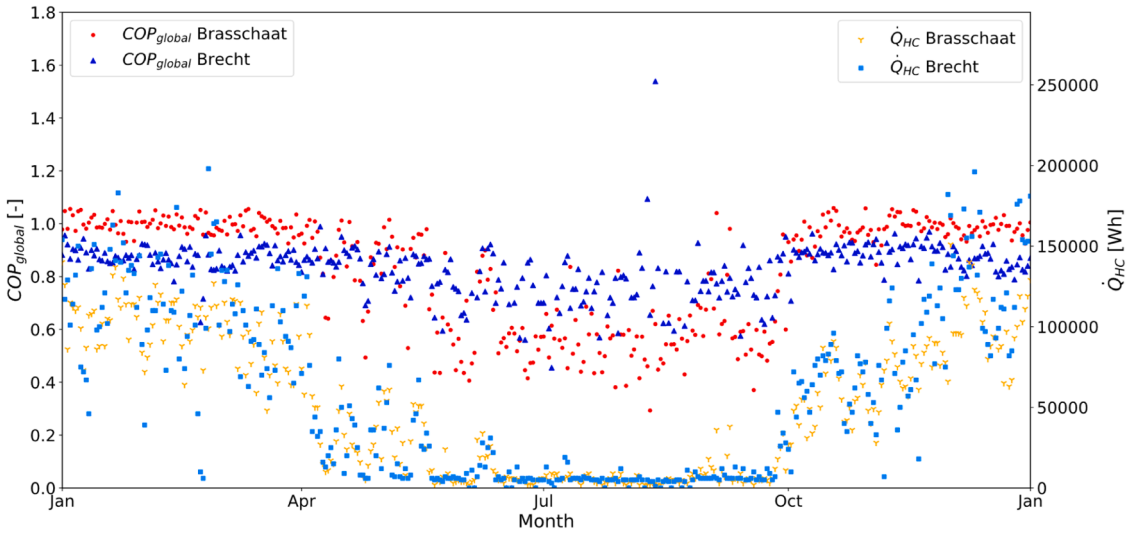

Fig. 6. Monitored GAHP's daily thermal production during 2020.

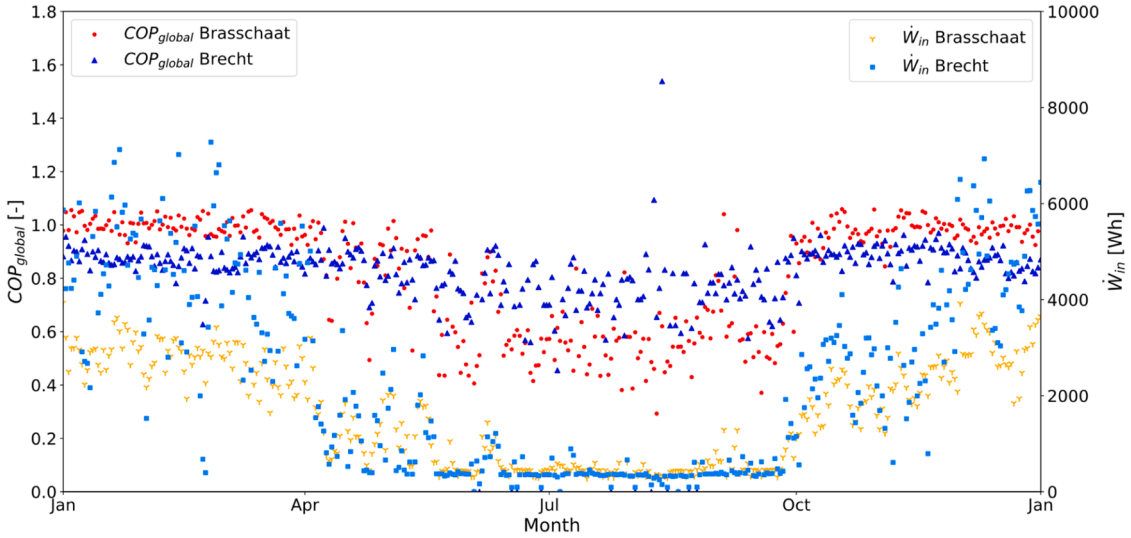

Fig. 7. Monitored GAHP's daily electrical consumption during 2020.

placed since the beginning, the installation was not significantly affected by the interventions made in July; besides this, the coupling with thermal solar panels causes the return temperature range to be very broad suggesting less demanding working conditions. At Brecht in the other hand and as shown in Fig. 4, the thermal production is dispatched to a single buffer tank; thus, the installation is simpler and the intervention had a greater effect in terms of system behavior since the sonde was misplaced.

The previous analysis made for the daily and monthly performances shows that an improvement has been achieved on site during the studied period; the results, however, are far from those obtained in the laboratory.

This does not imply, nonetheless, that the appliances never worked with higher performance results. In an effort to be consistent with the methodology followed during the experimental laboratory campaign, a more detailed analysis is performed for the monitored sites.

Small windows of time are selected during the year under a series of criteria that allow to say that the appliances are working under full power regime during the analyzed period. These periods have a duration of five minutes each, equivalent to the sampling rate of the data. A window of time is valid for further analyze if:

1 Electric consumption: the difference between two consecutive measurements exists and is at least greater or equal than 27.5 Wh
2 Gas consumption: the difference between two consecutive measurements exists and is at least greater or equal than 0.11 m^3
3 Thermal production: the difference between two consecutive measurements is zero, and at least one of the terms is greater than zero; this ensures that a thermal production was achieved, and that it is the same at the beginning and at the end of the period studied

With this is possible to ensure that, for the selected period of time, the appliance has a consumption of natural gas and electricity equivalent to the minimum observed in the laboratory for full load operation; also, it can be said that the heat production observed is a result of these consumptions and not from the heat storage buffers since the index of the counters increases. Finally, if this heat production is the same at the beginning and at the end of the period, it could be assumed that the system worked those five minutes under the same conditions; in other words, and steady state can be assumed, considering also that the heat counter is placed directly in the depart and return pipes of the appliance and measures the instantaneous thermal power provided (not an index).

The results of the COP_{global} for years 2020 and 2021, for both sites, as

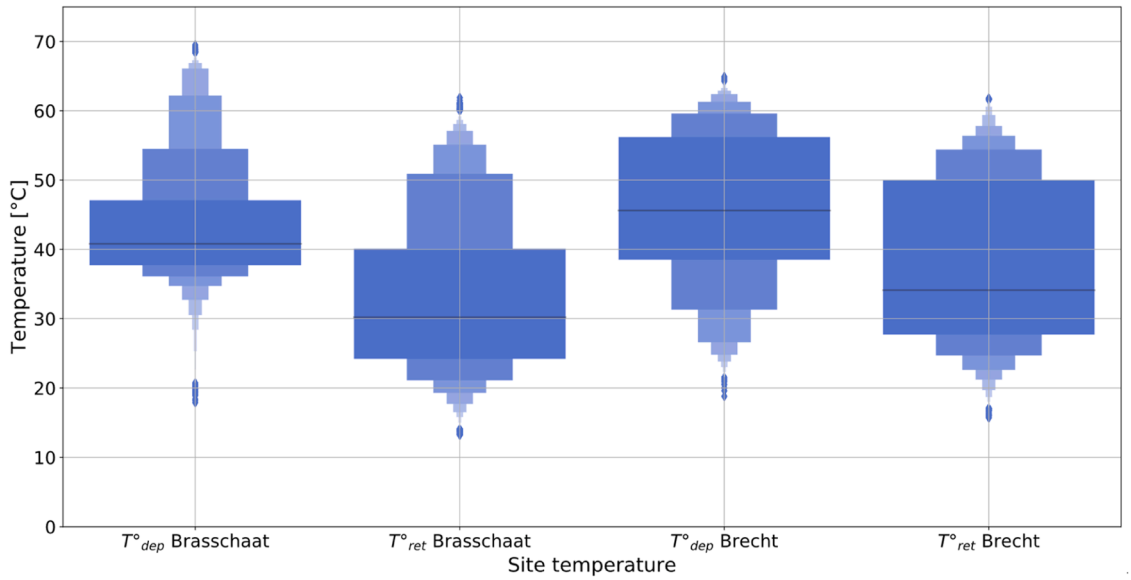

Fig. 8. Monitored GAHP's depart and return temperature during 2020.

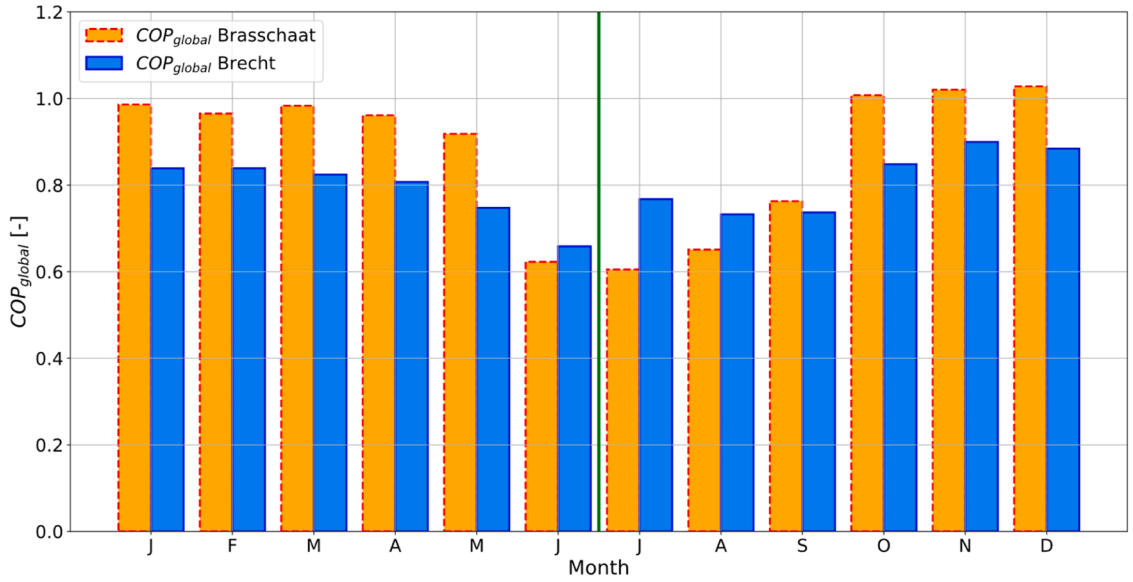

Fig. 9. Monitored GAHP's monthly COP_{global} during 2021.

a function of the outdoor temperature and water delivery temperature are summarized between Figs. 13 and 16. In Brasschaat during 2020 (Fig. 13), 3 COP_{global} outliers above 1.4 were discarded with the intention of homogenizing the y-axis scale and simplify the results comparison between sites. Those 3 outliers of a total of 258 points, represent the system warming up process where there is a delta $T°$ higher than 20 K and a peak of heating capacity is registered; thus, those points can be neither considered as a steady state period nor valid for further analysis. The same principle is applied for 1 outlier in 2021, of a total of 298 points in Fig. 14.

The results obtained for very low delivery temperatures at Brecht are also considered as outliers for similar reasons as the ones previously exposed. The low COP_{global} values obtained are result of conditions that fulfilled the valid windows criteria exposed in points 1, 2 and 3, but just with the minimum. The common point of these situations is a small heat production and a small water temperature difference between delivery and return of the appliance (~1–2 K), for gas and electricity inputs that are considered as full power regime during that window. Since the appliance is meant to work at higher temperatures (above 50 °C), those points cannot be considered as a steady state period or representative results of low delivery water temperatures. Nevertheless, these are only few points of the global (Fig. 15).

For Brasschaat site, the same reasoning can be applied but a wider range of temperatures could be accepted as valid since there are two temperature probes controlling the system (1 and 2 in Fig. 3), where the one corresponding to the SH control allows lower temperature operations.

The difference between the amount of points between sites that fulfill the imposed criteria is a direct cause of the control of the appliances and the coupling with other systems on site. At Brasschaat, less full load steady state points are found and at lower temperatures which shows that the GAHP is less thermally demanded compared to Brecht in terms of temperature regime (as shown in Figs. 8 and 12) and operation time; additionally, the coupling with thermal solar panels relieves the load imposed to the system, in contrast to Brecht where both the DHW and SH demands depend only on the GAHP. Nevertheless, since Brasschaat

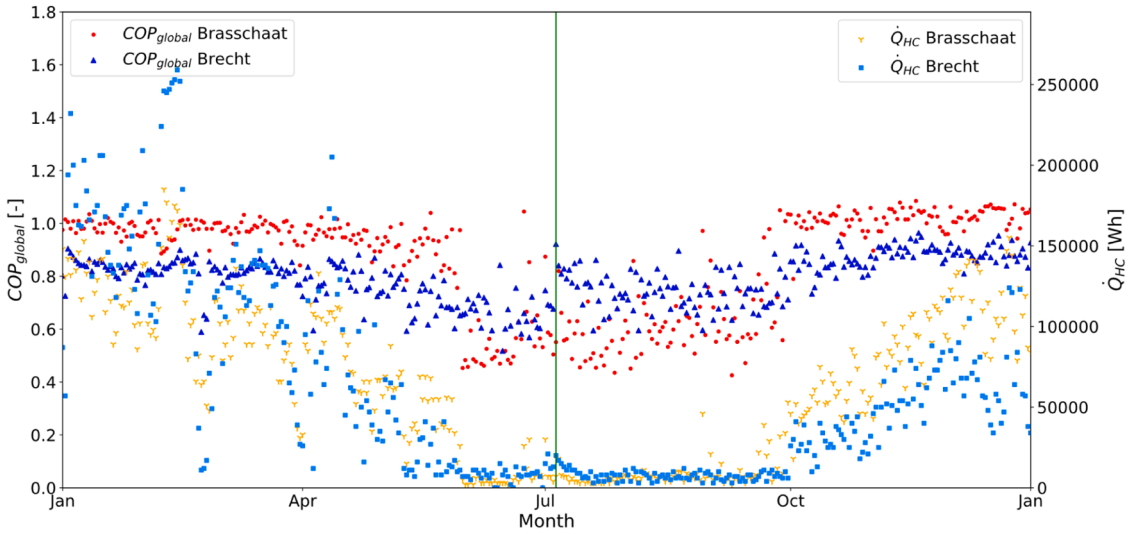

Fig. 10. Monitored GAHP's daily thermal production during 2021.

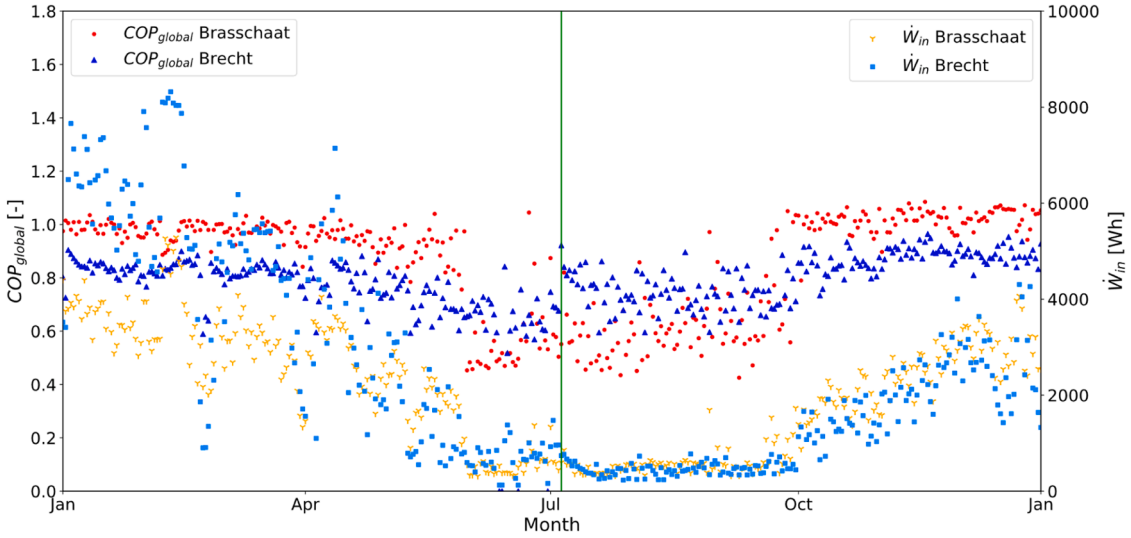

Fig. 11. Monitored GAHP's daily electrical consumption during 2021.

shows a better monthly behavior, the smaller amount of full load points proves that the system works more time under capacity modulation regime, leading to better overall results.

The field interventions had a less significant effect on the performance in Brasschaat than in Brecht, since 21 % of the points in Fig. 14 correspond to the period after intervention versus 67% in Fig. 16. In general terms, the trend in the COP_{global} in both sites regarding the outdoor temperatures is correct and in line with the laboratory results, that is to say, increasing as outdoor temperature does and vice versa. In terms of delivery water temperature a clearer effect can be observed in Brasschaat; since two temperature probes control the appliance, it is possible to identify two temperature levels in the results, while in Brecht only one high temperature level is noticeable with scattered results.

In any case, it is clear that the COP_{global} is more affected by the delivery water temperature than for the outdoor temperature. In general the field results are lower compared to those obtained in the laboratory, but there are points in which they approach to what is expected.

Modeling

An analysis of the data is carried out to define which variables influence the most the outputs of interest to model, and what is the shape of the data to define the model equations. The conclusions of this analysis are applied in this section to define the main guidelines of the model proposed.

From the experimental results, a simple model based on non-linear least squares curve fitting is developed; here, the optimal values for the parameters of each proposed equation are found in such a way that the sum of squared residuals is minimized as shown in Eq. (8).

$$\min \sum \| F(x_i) - y_i \|^2 \tag{8}$$

where $F(x_i)$ is a nonlinear function and y_i is independent data.

The model should give the Heating Capacity at full load ($\dot{Q}_{HC,FL}$) as a function of outdoor temperature (T_{out}) and delivery water temperature ($T_{delivery}$) as shown in Eq. (9). The global COP at full load ($COP_{Global,FL}$) depends on the same variables as shown in Eq. (10).

$$\dot{Q}_{HC,FL} = f\left(T_{out}, T_{delivery}\right) \tag{9}$$

$$COP_{Global,FL} = g\left(T_{out}, T_{delivery}\right) \tag{10}$$

A second test campaign is performed to collect data and information

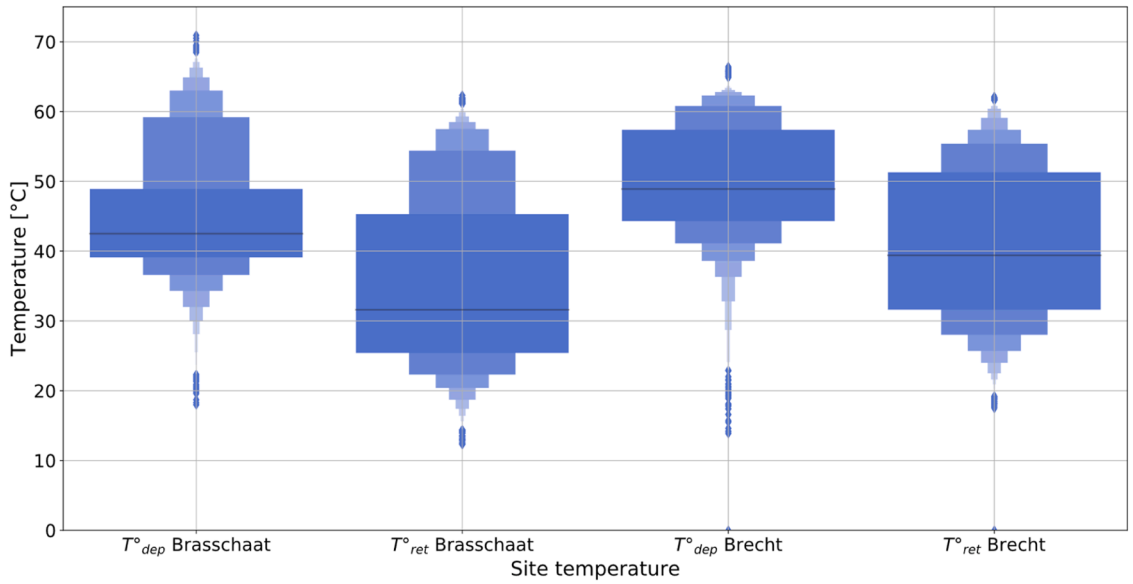

Fig. 12. Monitored GAHP's depart and return temperature during 2021.

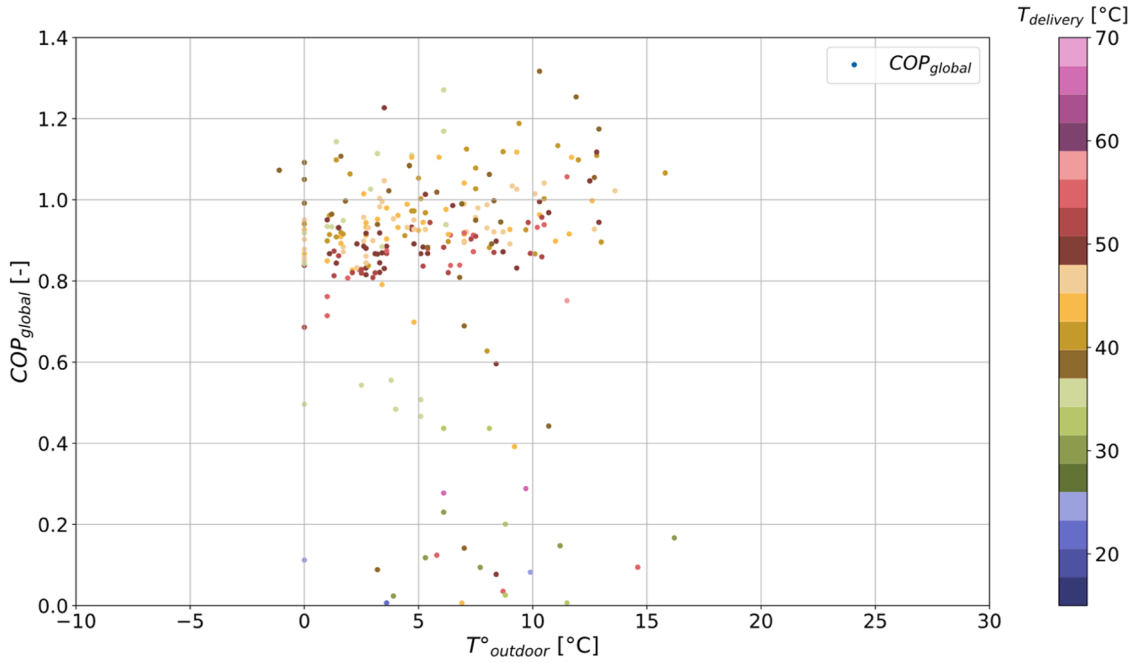

Fig. 13. COP_{global} for valid windows in Brasschaat during 2020.

regarding the behavior of the system at part load. This second round of experiments includes a hundred points and presents differences compared to the full load test campaign: it is performed for shorter test periods (not 20 min as before, but 3 to 5 min) and the focus is on understanding the behavior of the system while collecting data.

Variations of the thermal load imposed are made to record a variety of modulations. It is observed that during part load operation the heating capacity of the system changes thanks to the variation of the heating water flow made by the modulation of *WP* in Fig. 1. Variations on the inputs of the system are also found: the thermal input of the system is reduced through a reduction of the gas flow rate by the gas valve; in parallel, the combustion airflow is also reduced by a decrease of the combustion blower speed. These changes are reflected in the electricity consumption of the appliance, thus they must be considered in the model.

The part load ratio (*PLR*) is the ratio of the heating capacity at part load ($\dot{Q}_{HC,PL}$) to the heating capacity at full load as expressed in Eq. (11). This ratio is an input and must be a number between 0 and 1 since the heating capacity varies proportionally with the modulation of the system; this was verified with the experimental data.

$$PLR = \frac{\dot{Q}_{H,PL}}{\dot{Q}_{HC,FL}} \tag{11}$$

The gas heat input and electrical input are defined as $\dot{Q}_{gas}$ and $\dot{W}_{in}$ in Eqs. (12) and (13). The gas heat input varies according to the water delivery temperature and outdoor temperature, in addition to the modulation of the system; the electrical consumption is defined as a value that depends only on the modulation of the system, then, it is modeled as a function of the part load ratio and represented as a linear

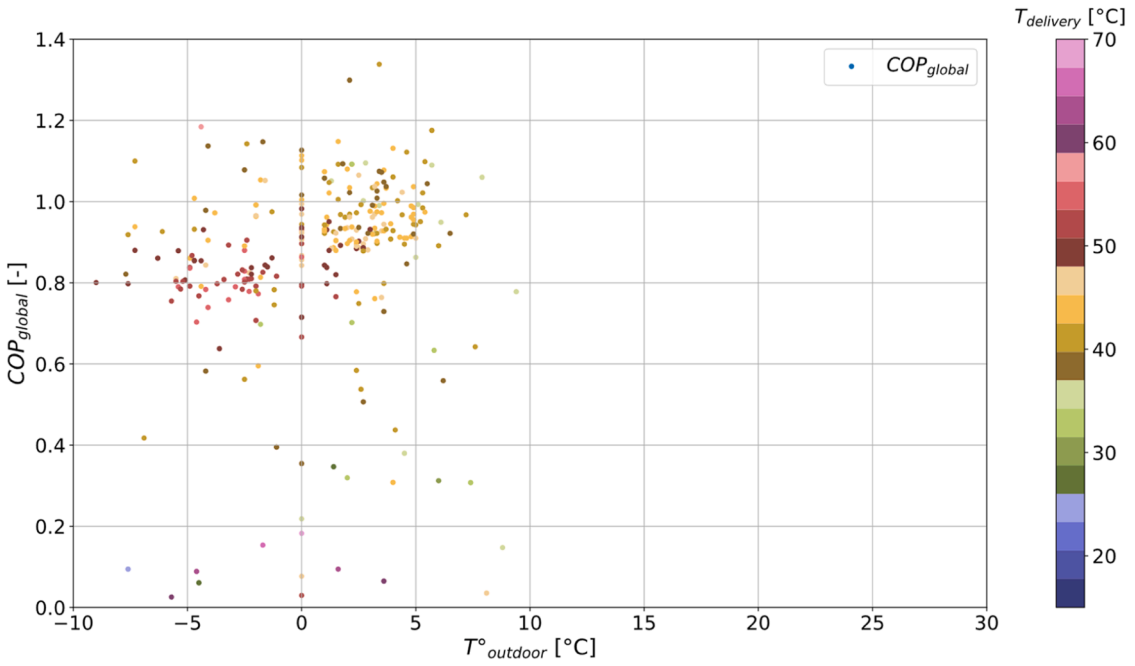

Fig. 14. COP_{global} for valid windows in Brasschaat during 2021.

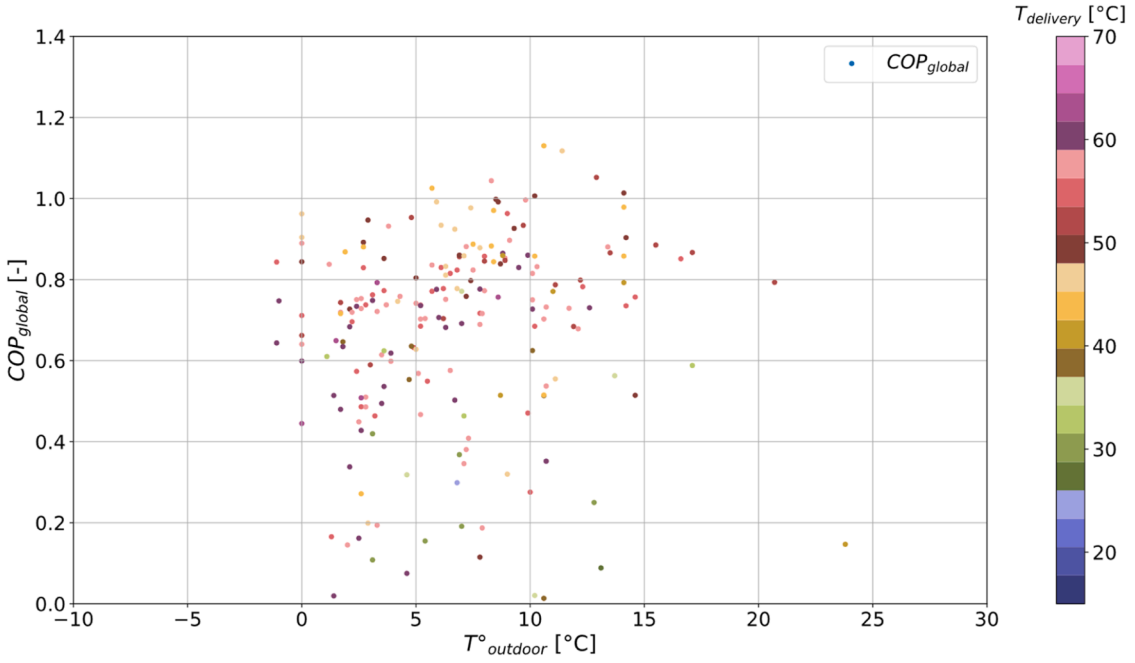

Fig. 15. COP_{global} for valid windows in Brecht during 2020.

proportion.

$$\dot{Q}_{gas} = h\left(T_{out}, T_{delivery}, PLR\right) \tag{12}$$

$$\dot{W}_{in} = i(PLR) \tag{13}$$

Based on this, the COP at part load (COP_{PL}) is computed based on the inputs and outputs at part load as shown in Eq. (14).

$$COP_{Global,PL} = \frac{\dot{Q}_{HC,PL}}{\dot{Q}_{gas} + \dot{W}_{in}} \tag{14}$$

With these statements and the experimental data available, a curve is fit. Boundaries are applied to be in line with the experimental trends. That is to say, the coefficients related to T_{out} should be positive and the ones related to $T_{delivery}$ negative for both, $\dot{Q}_{HC,FL}$ and $COP_{Global,FL}$; this ensures that both the COP and the heating capacity are adequately represented to increase as the outdoor temperature does, and decrease when the delivery temperature increases.

The results where the sum of squared residuals is minimized per equation are shown in Eqs. (15), (16), (17) and (18).

$$\dot{Q}_{HC,FL} = 0.12492\ T_{out} - 0.17745\ T_{delivery} + 25.30042 \tag{15}$$

$$COP_{Global,FL} = 0.00853\ T_{out} - 0.01106\ T_{delivery} + 1.68884 \tag{16}$$

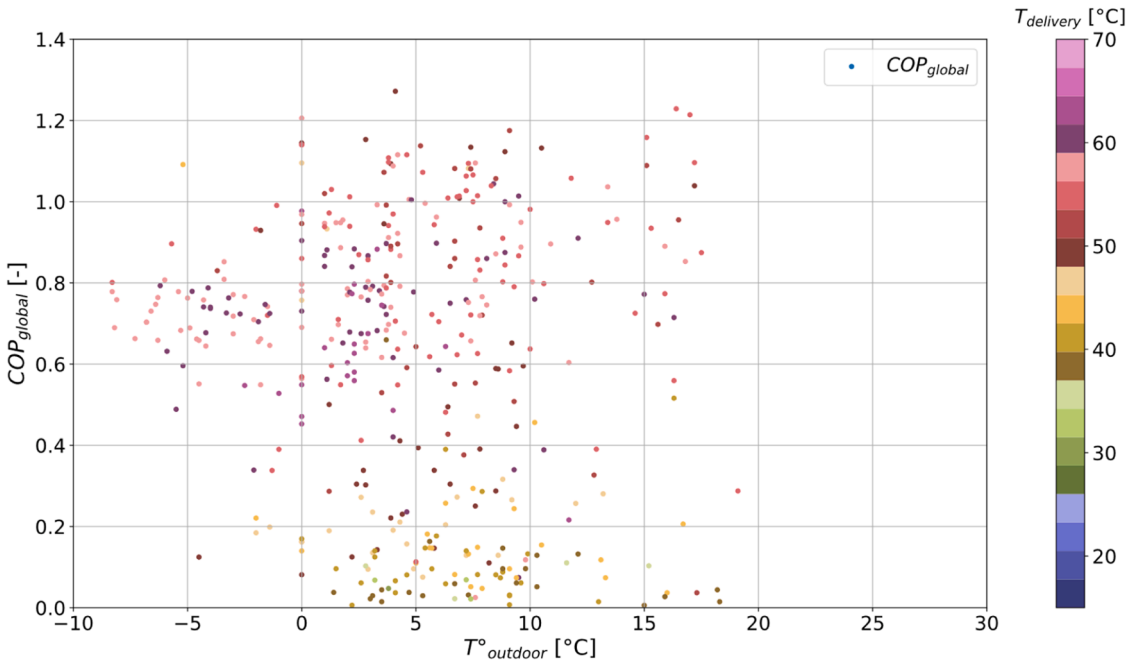

Fig. 16. COP_{global} for valid windows in Brecht during 2021.

$$\dot{Q}_{gas} = -0.00413 T_{out} - 0.01867\ T_{delivery} + 12.79157 PLR + 2.27197 \quad (17)$$

$$\dot{W}_{in} = 0.19390\ PLR^2 + 0.14844 \quad (18)$$

where T_{out} and $T_{delivery}$ are in [°C]; $\dot{Q}_{HC,FL}$, $\dot{Q}_{gas}$ and $\dot{W}_{in}$ are in [kW]; $COP_{Global,FL}$ and PLR are dimensionless. The parity plots to compare the model results against the experimental data per equation are shown in Fig. 17. It can be seen that most of the values are within the ±5 % range.

The model represents well the behavior in the laboratory, where the installation of the appliance and the control are in such a way as to obtain the best possible output. However, the model derived from laboratory data does not reflect the field behavior. This is due to the fact that the installations are different from the test bench in terms of control and coupling with other systems as shown in Figs. 3 and 4, reflected in poorer results in the field.

Therefore, a way is sought to penalize the COP and heating capacity for both field sites accordingly, based on the experimental model.

The same approach is used: a non-linear least squares curve fitting is used with sum of squared residuals minimization. The data found at full capacity from the small windows of time in the field is used and applied to the laboratory model, but now aiming to find a penalty factor for installation, in the form:

$$\dot{Q}_{HC,FL} = \left(a * T_{out} - b * T_{delivery} + c\right) * F_{inst,HC}, \quad 0 < F_{inst,HC} \leq 1$$

$$COP_{Global,FL} = \left(a * T_{out} - b * T_{delivery} + c\right) * F_{inst,COP}, \quad 0 < F_{inst,COP} \leq 1$$

where *a, b* and *c* are the coefficients obtained for Eqs. (15) and (16) respectively, and 1 representing an installation factor equivalent to the laboratory conditions. Based on the data analyzed per site, the results for the installation factor of each equation are in the form shown in 19 and 20 since the thermal production of each site decreases as shown in Fig. 10 with respect to the laboratory results, just like the COP does. Also and as stated before, since two temperature probes are used in Brasschaat, the control and results of this site are better than in Brecht, positioning the latter as the worst result expected.

$$\dot{Q}_{HC,FL} \rightarrow F_{inst,HC,Brecht} < F_{inst,HC,Brasschaat} < F_{inst,HC,laboratory} \quad (19)$$

$$COP_{Global,FL} \rightarrow F_{inst,COP,Brecht} < F_{inst,COP,Brasschaat} < F_{inst,COP,laboratory} \quad (20)$$

The results of the penalty factors found are shown in Table 8. Here it can be seen that more demanding operating conditions (i.e. higher temperature regime) along with non-optimal control can penalize the heating capacity and associated COP at full load conditions up to 47 %; a less demanding operation with better control on the other hand, could penalize the heating capacity and the COP in 18 % and 29 % respectively.

A comparison between the penalized model and the field sample data is shown from Figs. 18 to 21. It can be seen that the penalized factor per site applied to the experimental model reflects in an accurate way the behavior observed at Brasschaat for both, heating capacity and COP (Figs. 18 and 19). On the other hand, the characteristics of the installation, operating conditions and the bad control at Brecht are reflected in a dispersed behavior of the field data that is difficult to model, reason why the penalty factor is so large for this case (Figs. 20 and 21).

Conclusions

An experimental investigation of a gas absorption heat pump has been conducted where coefficients of performance have been calculated both in the laboratory and in the field, finding discrepancies between them being the latter lower than the former.

The results obtained in the laboratory confirm the expected trends, with performance that increase as the ambient temperature increases and decreases if the water outlet temperature increases. The orders of magnitude obtained correspond to those indicated by the manufacturer for the specified conditions.

For the monitored systems, a seasonal effect is clearly observed with global performance drops during the summer mainly related to the frequency of use of the systems and the impact on the thermal heat production. Both machines show not negligible differences between them of at least 10 percentage points on their performance values, results that led to perform interventions in the field, having a greater impact on one site than the other.

Even though the conditions in the field are far from being stationary, an attempt has been made to find windows of time in the monitored data that reflect the conditions of steady state observed in the laboratory.

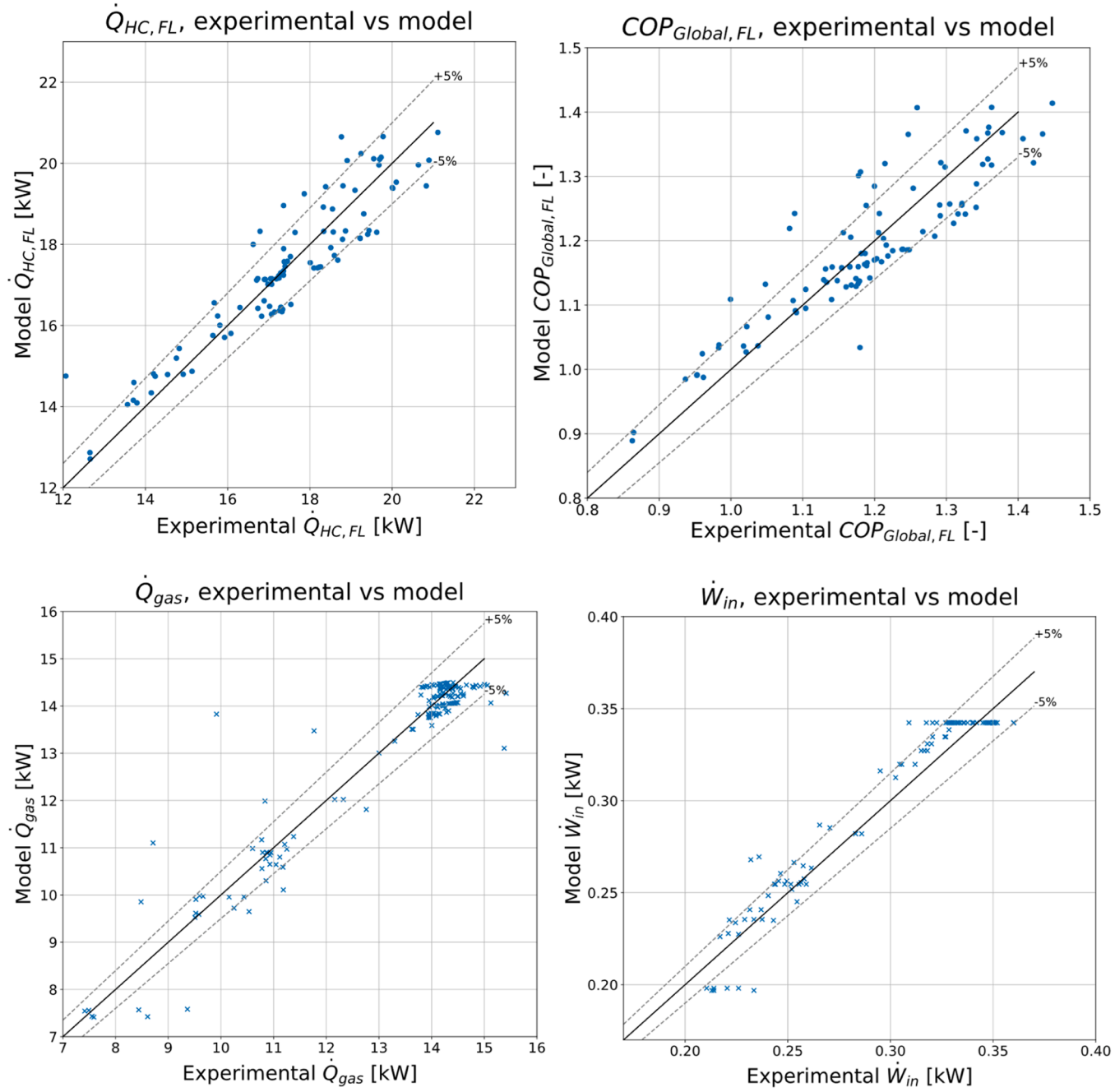

Fig. 17. Parity plots between experimental data and model results for: Heating Capacity at full load (top, left); Global COP at full load (top, right); Gas heat input (bottom, left); Electrical input (bottom, right).

Table 8
Penalty factor F_{inst} for heating capacity and COP.

$F_{inst,HC}$	$0.53 < 0.82 \leq 1$
$F_{inst,COP}$	$0.53 < 0.71 \leq 1$

Criteria regarding gas consumption, electricity consumption and heat production are considered to state a full load regime; delivery water temperature and outdoor temperature are considered to compute the global coefficient of performance.

In general terms, the field performances are still far from those obtained in the laboratory, but there are points in which they approach to what is expected. The results show that the combination of the working temperature regime, operation time, appropriate control for the specific application, proper installation of the system and consideration of coupling with other heat generation systems have led to significant differences on the resulting global coefficient of performance.

An experimental model is proposed to compute performance estimators based on the working temperature conditions (outdoor temperature, water delivery temperature) and operation regime (full load, part load). The experimental model represents in a proper way the behavior of the system in a facility where the goal is to get the best possible results, with most of the values within 5 % error.

The experimental model is then used to obtain a penalized model that includes a penalty factor based on the field results. This penalized model turns out to be more accurate for one facility than the other mostly due to the spread nature of the data caused by a poor control. The proposed penalty factor is mostly related to the quality of the appliance

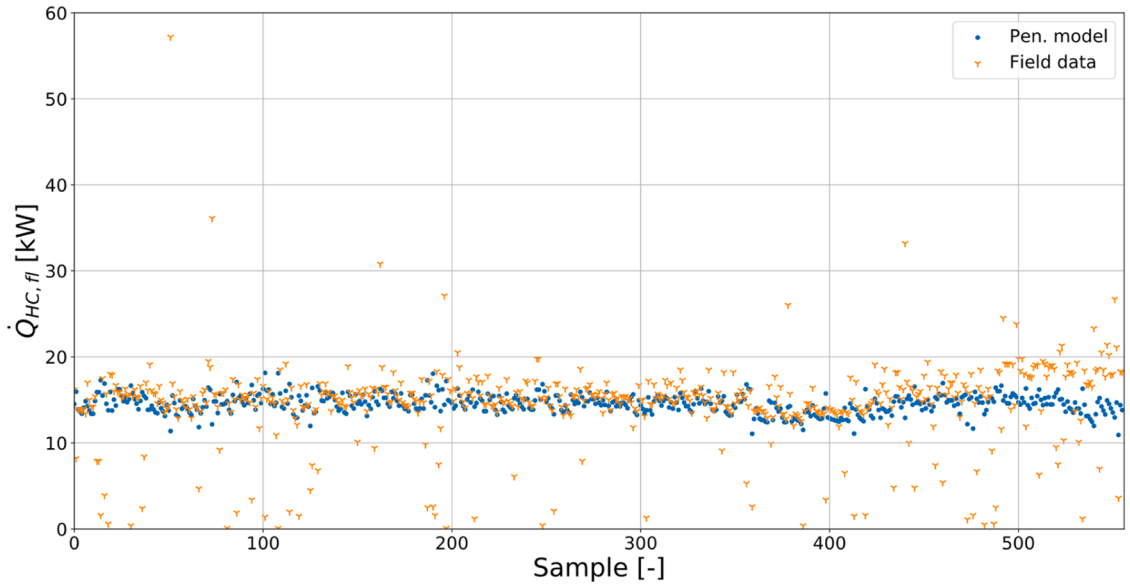

Fig. 18. Penalized model vs. field data samples for Heating Capacity at full load at Brasschaat.

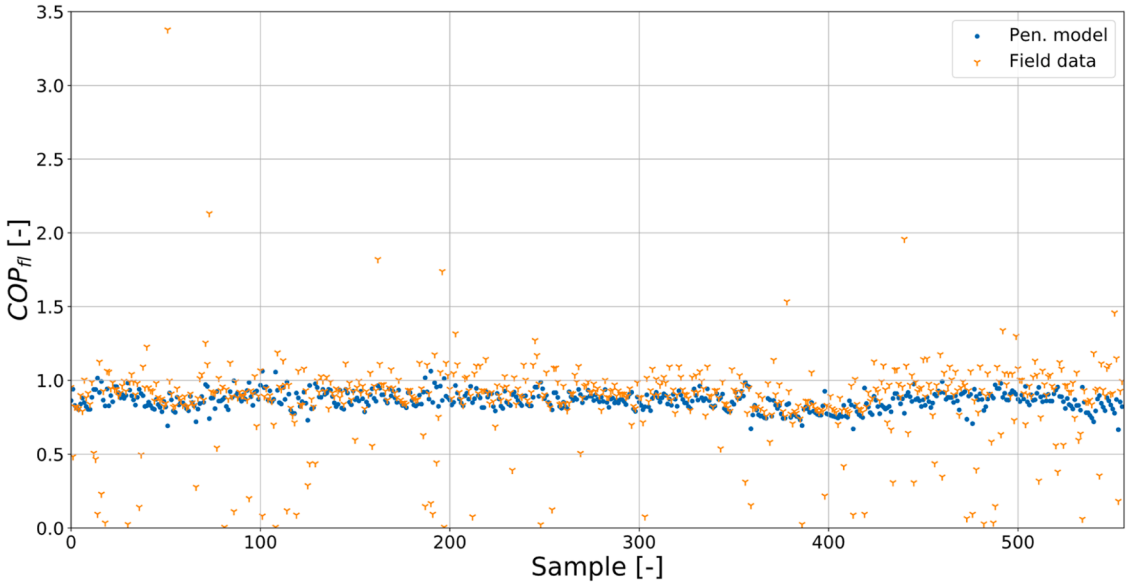

Fig. 19. Penalized model vs. field data samples for COP at full load at Brasschaat.

control for a higher delivery temperature regime, resulting in a decrease in the heating capacity which can vary between 18 % and 47 %; with respect to the COP, it can be penalized between 29 % and 47 %.

The few available information related to the monitored appliances and the low frequency sample rate of the measurement devices is a limitation of this work. Assumptions based on experimental observations had been made and applied to the field data in order to make possible a comparison between the two, limiting the accuracy of the results and the level of analysis that can be performed. Also, it is possible that the dynamics of the monitored sites differ from those observed in the laboratory and that not reported modification such as setpoint temperatures have taken place, affecting the behavior of the system and not being possible to detected them in the monitoring data.

Despite this, the presented results stress the differences found between the three studied facilities, highlighting the main role of proper installation and control not to diminish the main performance indicators such as the heating capacity and the COP.

CRediT authorship contribution statement

Camila Dávila: Conceptualization, Formal analysis, Investigation, Methodology, Writing – original draft. **Javier Vega:** Conceptualization. **Vincent Lemort:** Conceptualization, Funding acquisition, Supervision, Writing – review & editing.

Declaration of Competing Interest

The authors declare the following financial interests/personal relationships which may be considered as potential competing interests:

Camila Davila reports financial support was provided by Gas.be. Camila Davila reports financial support was provided by University of Liege.

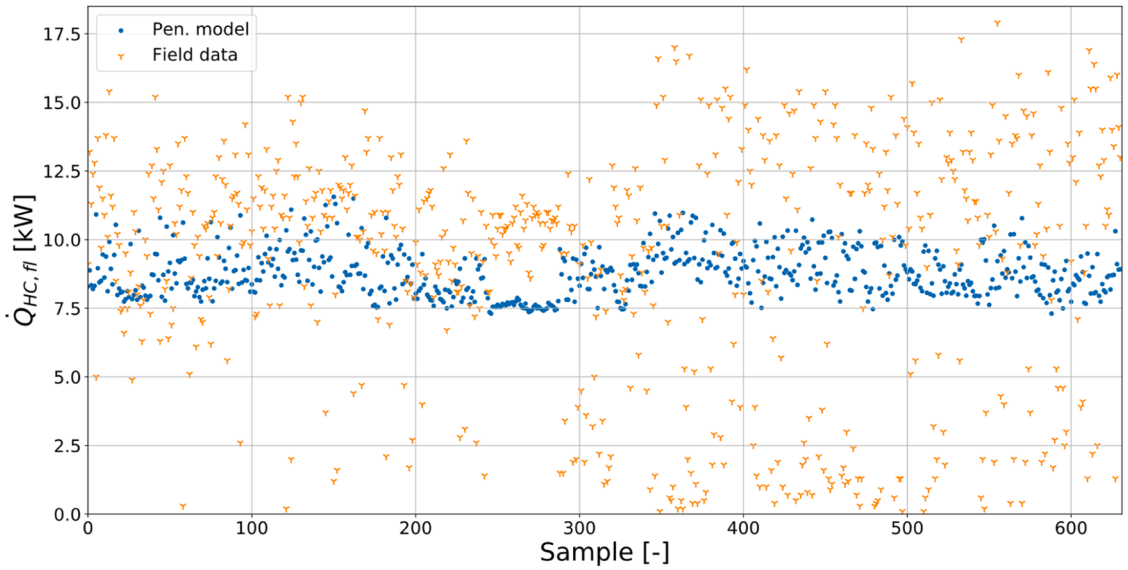

Fig. 20. Penalized model vs. field data samples for Heating Capacity at full load at Brecht.

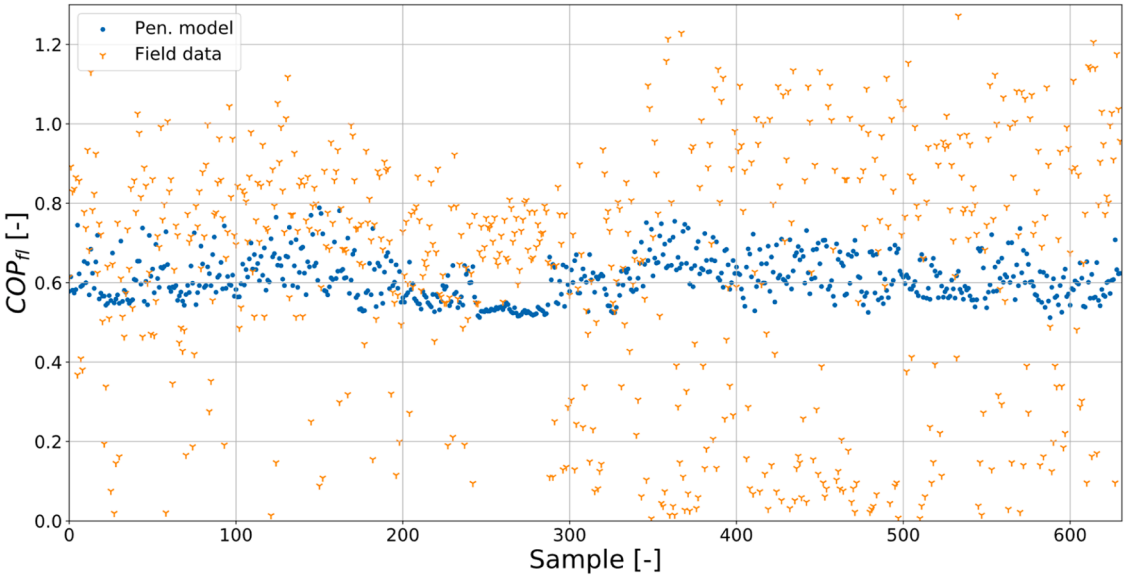

Fig. 21. Penalized model vs. field data samples for COP at full load at Brecht.

Data availability

The data that has been used is confidential.

Acknowledgments

The authors thank Gas.be for the financial support to this research project; thanks to Nicolas Paulus for the monitoring data provided.

References

Aprile, M., Scoccia, R., Toppi, T., Guerra, M., Motta, M., 2016. Modelling and experimental analysis of a GAX NH_3–H_2O gas-driven absorption heat pump. Int. J. Refrig. 66, 145–155. https://doi.org/10.1016/j.ijrefrig.2016.02.008.

Aprile, M., Scoccia, R., Toppi, T., Motta, M., 2017. Gray-box entropy-based model of a water-source NH_3-H_2O gas-driven absorption heat pump. Appl. Therm. Eng. 118, 214–223. https://doi.org/10.1016/j.applthermaleng.2017.02.099.

Aste, N., Adhikari, R.S., Manfren, M., 2013. Cost optimal analysis of heat pump technology adoption in residential reference buildings. Renew. Energy 60, 615–624. https://doi.org/10.1016/j.renene.2013.06.013.

Babak Dehghan, B., Toppi, T., Aprile, M., Motta, M., 2020. Seasonal performance assessment of three alternative gas-driven absorption heat pump cycles. J. Build. Eng. 31, 101434 https://doi.org/10.1016/j.jobe.2020.101434.

Belgium natural gas security policy. International Energy Agency. https://www.iea.org/articles/belgium-natural-gas-security-policy (accessed 16 October 2022).

Blarke, M.B., 2012. Towards an intermittency-friendly energy system: comparing electric boilers and heat pumps in distributed cogeneration. Appl. Energy 91, 349–365. https://doi.org/10.1016/j.apenergy.2011.09.038.

Chua, K.J., Chou, S.K., Yang, W.M., 2010. Advances in heat pump systems: a review. Appl. Energy 87, 3611–3624. https://doi.org/10.1016/j.apenergy.2010.06.014.

Energy technology perspectives, Clean energy technology guide. International Energy Agency. https://iea.blob.core.windows.net/assets/355d9b26-b38c-476c-b9fa-0afa34742800/iea_technology-guide-poster.pdf. (accessed 16 October 2022).

European Environment Agency, 2013. Total final energy consumption by sector in the EU-27, 1990–2010. Retrieved from Total final energy consumption by sector in the EU-27, 1990–2010.

European Environment Agency, 2016. Energy consumption by end use per dwelling. Retrieved from Energy consumption by end use per dwelling.

European Environment Agency, 2020. Final energy consumption by fuel type and sector. Retrieved from Growth in renewable energy use by technology and sector, 2005-2018.

European Environment Agency, 2020. Growth in renewable energy use by technology and sector, 2005-2018. Retrieved from Final energy consumption by fuel type and sector.

European Standards, 2014. Gas-fired sorption appliances for heating and/or cooling with a net heat input not exceeding 70 kW.

Executive summary Belgium 2022. International Energy Agency. https://www.iea.org/reports/belgium-2022/executive-summary (accessed 16 October 2022).

Famiglietti, J., Toppi, T., Pistocchini, L., Scoccia, R., Motta, M., 2021. A comparative environmental life cycle assessment between a condensing boiler and a gas driven absorption heat pump. Sci. Total Environ. 762, 144392 https://doi.org/10.1016/j.scitotenv.2020.144392.

Fuels: old and new. International Energy Agency. https://www.iea.org/reports/world-energy-outlook-2021/fuels-old-and-new (accessed 16 October 2022).

Fumagalli, M., Sivieri, A., Aprile, M., Motta, M., Zanchi, M., 2017. Monitoring of gas driven absorption heat pumps and comparing energy efficiency on primary energy. Renew. Energy 110, 115–125. https://doi.org/10.1016/j.renene.2016.12.058.

Heating. International Energy Agency. https://www.iea.org/reports/heating (accessed 16 October 2022).

Hommelberg M., Janssen G., Friedel P., 2022. Installatiemonitor: praktijkpresentaties van warmtepompen. https://www.installatiemonitor.nl/wp-content/uploads/2022/02/Eindrapportage-Installatiemonitor-v2.1.pdf.

IEC 62053-21, 2003. Electricity metering equipment (a.c.) – Particular requirements. Part 21 : static meters for active energy (classes 1 and 2). International Electrotechnical Commission.

Keinath, C.M., Srinivas, G., 2017. An energy and cost comparison of residential water heating technologies. Energy 128, 626–633. https://doi.org/10.1016/j.energy.2017.03.055.

OIML R 49-1, 2006. Water Meters Intended for the Metering of Cold Potable Water and Hot Water. Part 1: Metrological and Technical Requirements. International Organization of Legal Metrology.

Paulus, N., Lemort, V., 2022. Establishing the energy content of natural gas residential consumption: example with Belgian field-test applications. In: Proceedings of the 8th Conference of the Sustainable Solutions for Energy and Environment (EENVIRO 2022).

Weather Underground. https://www.wunderground.com/dashboard/pws/IARRONDI6/table/2018-12-9/2018-12-9/daily (accessed March 2020).

Wu, Z., You, S., Zhang, H., Wang, Y., Wei, S., Jiang, Y., Sha, L., 2020. Performance analysis and optimization for a novel air-source gas-fired absorption heat pump. Energy Convers. Manag. 223, 113423 https://doi.org/10.1016/j.enconman.2020.113423.